

EFFECTS OF SIMULATED MICROGRAVITY ON SENESCENT HUMAN FIBROBLASTS

Ly Ngoc Cang^{1,2}, Hoang Nghia Quang Huy¹, Hoang Nghia Son¹, Le Thanh Long^{1,*}

¹Institute of Tropical Biology, VAST, Vietnam

²University of Science, Vietnam National University of Ho Chi Minh City, Vietnam

Received 20 December 2021; accepted 6 June 2022

ABSTRACT

This study aimed to assess the effects of simulated microgravity (SMG) on senescent human fibroblasts (HFs). The HFs were treated with 150 µM H₂O₂ in a culture medium for 90 minutes for senescent induction. The senescent HFs were induced SMG for 72 hours by a Gravity simulator, while the control group was treated in the same CO₂ incubator. Cell morphology analysis showed that the SMG condition retrieved the fibroblastic morphology from the senescence. WST1 assay and cell counting indicated that the senescent HFs viability from the SMG group was higher than the control group (OD value of 0.80 ± 0.13 vs. 0.64 ± 0.11, respectively). In cell cycle progression, the G0/G1 cell percentage of senescent HFs from the SMG group was reduced, compared to the control group (45.84 ± 1.37% vs. 57.22 ± 1.56%, respectively). The senescent HFs from the SMG group exhibited a lower nuclear area than the control group (186 ± 4 µm² vs. 217 ± 8 µm², respectively). This resulted in the performance of a higher nuclear shape value of senescent HFs from SMG, compared to the control group (0.74 ± 0.02 vs. 0.70 ± 0.01, respectively). SMG condition caused the down-regulation of the senescence-related transcript. These results found that SMG could regain the normal characteristics of HFs from the senescence.

Keywords: cell cycle, cell viability, human fibroblast, senescence.

Citation: Ly Ngoc Cang, Hoang Nghia Quang Huy, Hoang Nghia Son, Le Thanh Long, 2022. Effects of simulated microgravity on senescent human fibroblasts. *Academia Journal of Biology*, 44(2): 115–122.
<https://doi.org/10.15625/2615-9023/16836>

*Corresponding author email: lelongvast@gmail.com

©2022 Vietnam Academy of Science and Technology (VAST)

INTRODUCTION

Cellular senescence is a term used to describe a state of permanent cell cycle arrest in cells grown in culture (van Deursen, 2014; Kumari & Jat, 2021). This cell response was later identified *in vitro* and *in vivo* for cells exposed to various types of stress. It has more recently been implicated in physiological situations during development. The first study of cell senescence was conducted on human primary fibroblasts in order to determine the best cell culture conditions (Hayflick & Moorhead, 1961). The goal was to establish a reliable source of human cells that could be exploited for vaccine development and other biotechnological purposes. Early cell culture technologies used existing cell lines taken from human and animal. Human primary fibroblasts could be adapted to *in vitro* cell culture conditions and proliferated at a consistent rate during the early stages of the culture, in contrast to the tumor cells' robust and permanent proliferation (Da Silva-Álvarez & Collado, 2016). Cells shifted to a flattened and expanded appearance as cultures accumulated passages, and they ceased to proliferate (González-Gualda et al., 2021). Since the addition of additional growth factors did not result in the resumption of cell division, the growth arrest remained stable. These findings lead the authors to link cell senescence to the aging process. Proliferative exhaustion was seen as the cellular reflection of organismal decay. Tumor cells, on the other hand, were immortal and showed no properties of aging. One important conclusion drawn from this theoretical framework is that cells require a counting mechanism to initiate the senescence process (Da Silva-Álvarez & Collado, 2016).

Numerous studies have shown that SMG has significant effects on cell physiology, such as reducing cell proliferation *in vitro*, altering the cell cycle, and changing cytoskeleton structure (Lei et al., 2018; Grimm et al., 2020; Degan et al., 2021; Ho et al., 2021). SMG has been shown to have a marked effect on the cell's ability to differentiate (Li et al., 2021). Furthermore,

cell viability was also affected by SMG (Martinelli et al., 2009; Vidyasekar et al., 2015). However, the effects of SMG on cell senescence have not been well characterized. Therefore, this study was conducted to estimate the changes of senescent HFs under SMG conditions. The senescent characteristics were assessed to clarify the alterations in senescent HFs induced by SMG, such as the changes in HFs morphology, viability, cell cycle progression, and the transcript expression of the senescence-related gene.

MATERIALS AND METHODS

Cell culture and senescence induction

The HFs were cultured in T25 flask with 5 mL culture medium containing DMEM/Ham's F-12 (Capricorn Scientific, Germany), with 15% FBS (Capricorn Scientific, Germany) and 1% Pen/Strep (Capricorn Scientific, Germany) at 37 °C, 5% CO₂. The senescence induction of HFs was performed with 150 µM H₂O₂ in a culture medium for 90 minutes. The HFs were washed with PBS three times in 5 min for each step. The senescent HFs was induced SMG for 72 h by Gravity Controller Gravite® (AS ONE INTERNATIONAL, INC., Santa Clara, CA, United States) (Ho et al., 2021). The cell plate and flask of the control group were cultured in the same CO₂ incubator.

WST-1 Assay

The HFs viability was estimated by WST-1 assay (Son et al., 2019). The HFs were seeded in 96-well plates at a density of 1×10^3 cells/well and induced SMG for 72 h. After 72 h, the medium was removed. 100 µl fresh cell culture medium and 10 µl WST-1 solution (Roche, Switzerland) was added to each well and incubated at 37 °C, 5% CO₂ for 3.5 h. The Optical Density 450 (O.D. 450) value was measured by GloMax® Microplate Reader (Promega, United States).

The cell density determination and cell cycle progression analysis

The HFs were fixed with 4% paraformaldehyde for 30 min and

permeabilized with 0.1% Triton X-100 in PBS for 30 min. The nuclei were stained with Hoechst 33342 (Sigma-Aldrich, United States) for 30 min. Cell washing with PBS was applied three times in 5 min for each step. Cell number and cell cycle progression were determined by nuclei counting with Cell Cycle App. of Cytell microscope (GE Healthcare, United States) (Ho et al., 2021).

Quantitative real-time RT-PCR

Total RNA was extracted by a ReliaPrep™ RNA Cell Miniprep System (Promega, USA). Each reaction was carried

out in 20 μ L reaction including 1 μ L of total RNA, 2 μ L of primers (forward and reverse), 10 μ L 2X Mix Hi-ROX, 1 μ L RTAse, and 6 μ L dH₂O. The qRT-PCR reaction was performed by one cycle of 45 °C for 15 min, one cycle of 95 °C for 2 min, 40 cycles of 95 °C for 10 sec, 60 °C for 15 sec and 71 cycles of 60 °C for 15 sec. PikoReal 96 Real-Time PCR System (Thermo Scientific, United States) was used for qRT-PCR with 2x qPCR SyGreen 1-Step Go Hi-ROX kit (PCR Biosystem, England). The $2^{-\Delta\Delta Ct}$ method was applied for Ct value analysis. Primers were presented in Table 1.

Table 1. Primers for quantitative real time RT-PCR

Gene	Primer sequence	Reference
p53	F: 5'-GAG CAC TGC CCA ACA ACA C-3'	Chen et al., 2012
	R: 5'-ATG GCG GGA GGT AGA CTG A-3'	
p16	F: 5'-TGA GCA CTC ACG CCC TAA GC-3'	Mavrogonatou et al., 2018
	R: 5'-TAG CAG TGT GAC TCA AGA GAA GCC-3'	
p21	F: 5'-TGG AGA CTC TCA GGG TCG AAA-3'	Mavrogonatou et al., 2018
	R: 5'GGC GTT TGG AGT GGT AGA AAT C-3'	
cyclin D	F: 5'- ATG TTC GTG GCC TCT AAG ATG A-3'	Li et al., 2016
	R: 5'- CAG GTT CCA CTT GAG CTT GTT C-3'	
Gapdh	F: 5'-GAA GGT CGG AGT CAA CGG ATT T-3'	Chen et al., 2012
	R: 5'-CTG GAA GAT GGT GAT GGG ATT TC-3'	

Nuclear morphology analysis

Cells were fixed with 4% paraformaldehyde for 30 min, then permeabilized with 0.1% Triton X-100 overnight at 4 °C. The nuclei were stained with Hoechst for 15 min. The cells were washed three times with PBS, 10 min each. The stained cells were observed under a Cytell microscope (GE Healthcare, United States). The Cell Cycle App of the Cytell microscope was applied to assess the nuclear morphology, including nuclear area and nuclear shape value (Ho et al., 2021).

Statistical analysis

The data were analyzed for statistical significance by one-way ANOVA where $P < 0.05$ was considered statistically significant.

RESULTS

SMG altered HF proliferation

The HFs from the SMG group showed a lower density than the control group (Fig. 1A). The HFs of the control group exhibited stronger senescent characteristics than the SMG group. The viability of HFs was assessed by WST-1 assay. As seen in Figure 1B, the OD value of HFs from the SMG group was 0.80 ± 0.13 which was higher than the control group (0.64 ± 0.11). However, the cell density of the control group was higher than the SMG group ($18,186 \pm 1,340$ cells/well vs. $14,106 \pm 621$ cells/well, respectively). This result showed that the SMG condition could retrieve the viability of HFs from the senescence.

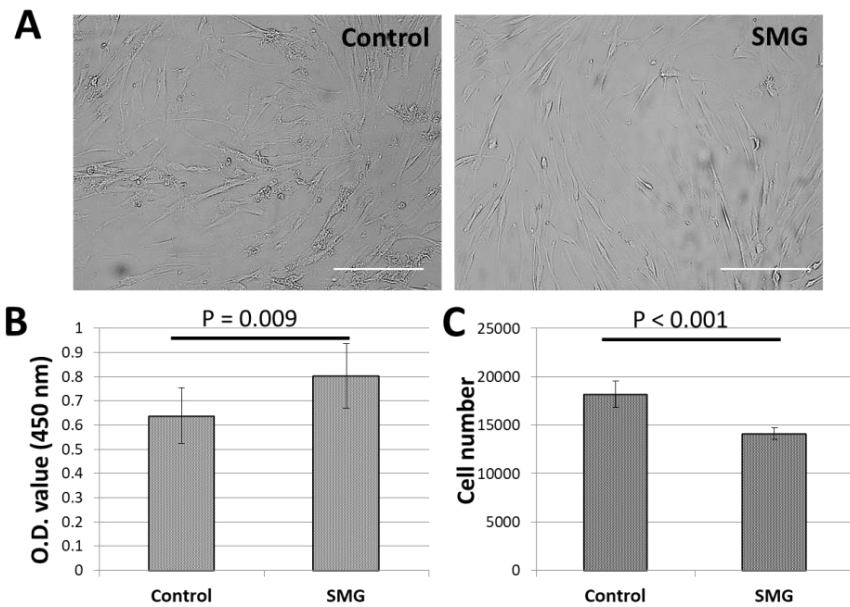


Figure 1. The proliferation of senescent HFs. A. HF morphology under control group and SMG condition. B. WST1 assay was applied to assess cell viability ($n = 10$). C. Cell number was performed by Cell cycle App ($n = 6$) of Cytell microscope. Scale bar = 223.64 μm

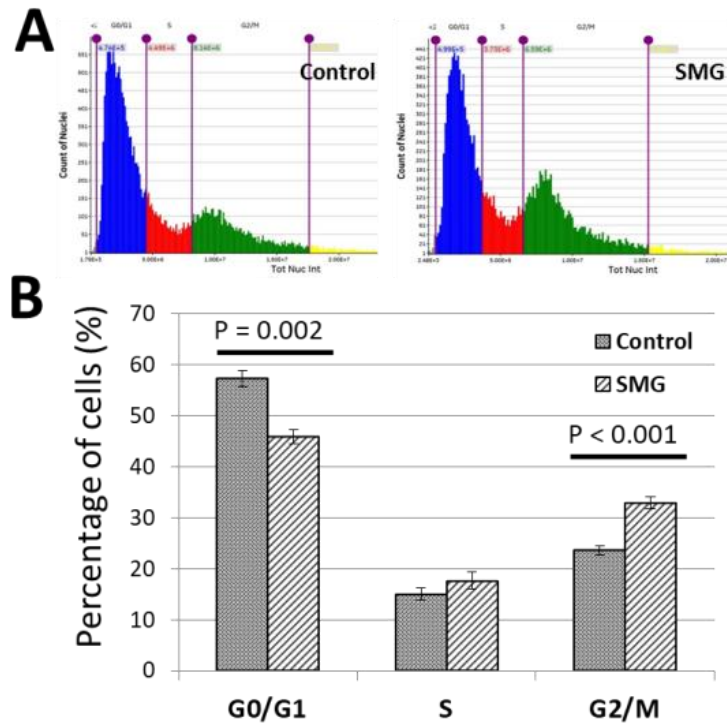


Figure 2. Cell cycle progression was analyzed by Cell cycle App. of Cytell microscope. A. Cell cycle progression of senescent HFs from the control group and SMG group (the blue indicates G0/G1 phase, the red indicates S phase, and the green indicates G2/M phase). B. The percentage of cells in cell cycle phases ($n = 4$)

The cycle progression of HFs was estimated by flow cytometry analysis (Figs. 2A, 2B). The percentage of HFs in the G0/G1 phase from the control group was higher than in SMG groups ($57.22 \pm 1.56\%$ vs. $45.84 \pm 1.37\%$, respectively). The percentage of HFs in the G2/M phase from the SMG group was higher than the control group ($32.94 \pm 1.12\%$ vs. $23.60 \pm 0.87\%$, respectively). This result indicated SMG condition induced an alteration in cell cycle progression of senescent HFs, demonstrated by reducing the percentage of HFs in the G0/G1 phase and increasing the percentage of HFs in G2/M.

SMG induced the changes in nuclear morphology

This study also evaluated the changes in nuclear morphology. The nuclear area of HFs from the control group was higher than SMG group ($217 \pm 8 \mu\text{m}^2$ vs. $186 \pm 4 \mu\text{m}^2$, respectively) (Fig. 3A). The nuclear shape value (1.0 = circle, < 1.0 = non-circular), was also applied to evaluate the nuclear morphology of HFs. The result showed that HFs from the SMG group exposed a higher nuclear shape value than the control group (0.74 ± 0.02 vs. 0.70 ± 0.01 , respectively). As shown in Figure 3C, the SMG group showed a lower distribution of nuclear area than the control group. In contrast, HFs from the SMG group showed a higher distribution of nuclear shape values than the control group (Fig. 3D).

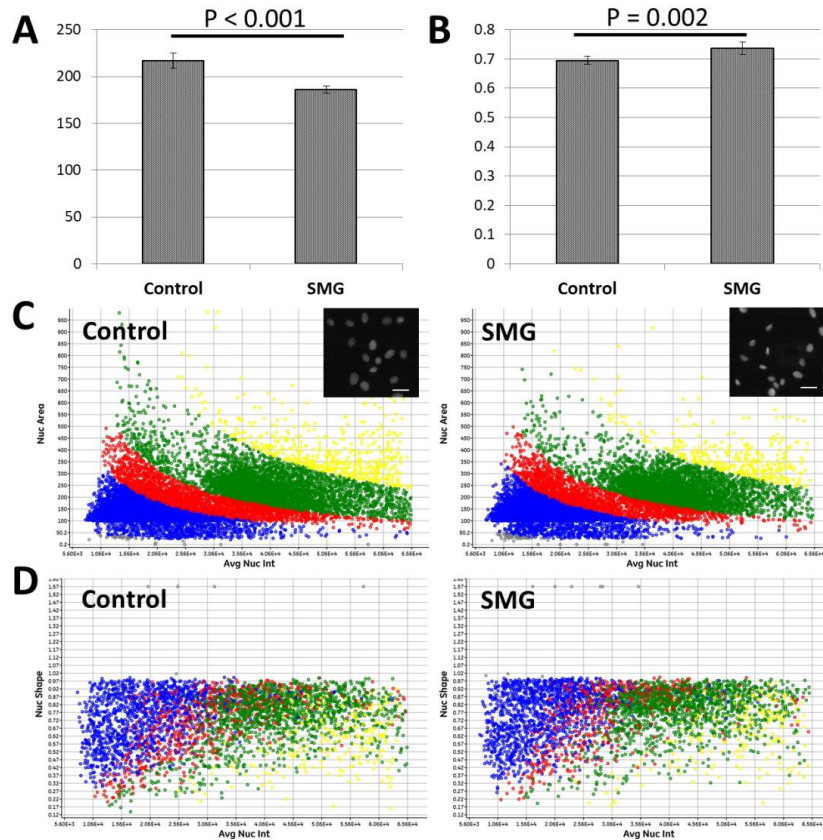


Figure 3. Nuclear morphology analysis. A. Nuclear area analysis of senescent HFs (n = 6). B. Nuclear shape value analysis of senescent HFs (n = 6). C. The distribution of the nuclear area in the relation to nuclear intensity, the nuclei were stained with Hoechst 33342, Scale bar = 10 μm. D. The distribution of nuclear-shape values in relation to nuclear intensity. Blue colour indicates the G0/G1 phase, red indicates the S phase, green indicates the G2/M phase, grey indicates <2n and yellow indicates >4n

SMG reduced the transcript expression of the senescence-related gene

In this investigation, real time RT-PCR was performed to estimate the transcript expression of the senescence-related gene. Figure 4 demonstrated that the transcript expression of p53 in HF from the SMG group was lower than in the control group.

HFs from the SMG group exhibited the down-regulation of p16 and p21, compared to the control group. In addition, the marked reduction of cyclin D was also observed HF from the SMG group. These results revealed that the SMG condition induced the attenuation of transcript expression of the senescence-related gene in senescent HFs.

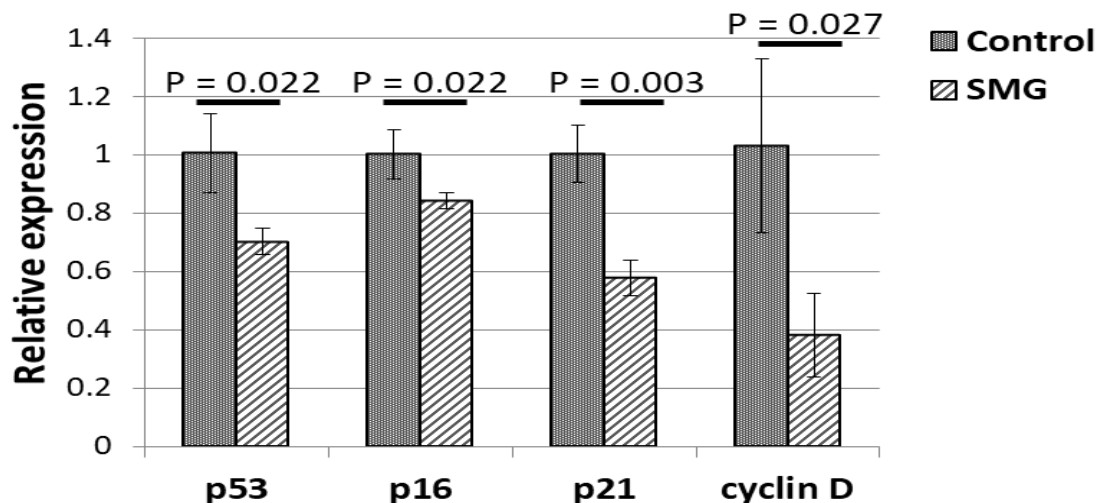


Figure 4. Real time RT-PCR analysis. HFs from SMG showed the transcript reduction of the senescence-related gene, compared to the control group ($n = 3$)

DISCUSSION

The morphology of human diploid fibroblasts changes from a spindle shape to an enlarged, flattened, and irregular shape during cellular senescence. It plays a crucial role in many cellular processes concluding migration, differentiation, apoptosis, necrosis and senescence (Chen et al., 2000). In this study, the senescent HFs from the control group maintained the senescent morphology for 3 days such as irregular shape, cytoplasmic fragmentation, whereas SMG-induced HFs regained the fibroblastic morphology and reduced the fragmentation. This suggested that the SMG condition could retrieve fibroblastic morphology from senescence.

The previous study demonstrated that SMG induces the inhibition of cell proliferation (Quynh Chi et al., 2020; Ho et al., 2021). In this study, senescent HFs from the SMG group showed a lower proliferation than

the control group. However, the senescent HFs showed higher viability under SMG conditions, compared to the control group. This revealed that SMG could recover the viability of senescent HFs.

Senescence was classically defined as an irreversible cell cycle arrest in the G1 phase (G1 exit) triggered by eroded telomeres in aged primary cells (Gire & Dulić, 2015; Wang et al., 2020). The present work indicated that the cell ratio of the G0/G1 phase from the SMG group was lower than the control group, suggesting that SMG conditions induce a reduction of the G0/G1 ratio and prevent HFs from the cell cycle arrest phase.

The senescent cells exhibited the nuclear enlarge, loose their shape, appear lobulated, harbor nuclear membrane invaginations, carry enlarged/fragmented nucleolus, loose heterochromatin (Pathak et al., 2021). The present investigation demonstrated that the

enlargement of HF's nuclear from the control group was stronger than the SMG group, demonstrated by the higher nuclear area. This led to the decrease in nuclear shape value in senescent HF's from the control group.

The most studied pathways involved in the regulation of cellular senescence are p53/p21 and/or p16/Rb tumor suppressor pathways (Sharpless & Sherr, 2015). p53 regulates the expression of a large number of target genes involved in cell cycle arrest, DNA repair, senescence, and apoptosis (Fischer, 2017). The p21 is capable of inactivating all CDKs, thereby inhibiting cell cycle progression (Wade Harper et al., 1993). The p16 mediated senescence acts through the retinoblastoma (Rb) pathway inhibiting the action of the cyclin dependent kinases leading to G1 cell cycle arrest. The previous study reported the up-regulation of p53, p16, and p21 gene in human fibroblasts (Alcorta et al., 1996; Stein et al., 1999). Moreover, the expression of cyclin D also increases in senescent human fibroblasts. In this work, the reduced expression of p53, p16, p21, and cyclin D was determined in HF's under SMG, suggesting that the SMG condition could attenuate the expression of the senescence-related transcript.

CONCLUSION

This study found that SMG induces the alterations in senescent HF's, demonstrated by retrieving the fibroblastic morphology, increasing senescent HF's viability, preventing senescent HF's from the cell cycle arrest phase, down-regulating the transcript expression of the senescence-related gene.

Acknowledgements: This work was supported by the Vietnam Academy of Science and Technology under the Grant of Senior Researcher. We would like to thank Dr. To Minh Quan, University of Science, Vietnam National University of Ho Chi Minh City for the gift of the human fibroblast.

REFERENCES

Alcorta D. A., Xiong Y., Phelps D., Hannon G., Beach D., Barrett J. C., 1996.

Involvement of the cyclin-dependent kinase inhibitor p16 (INK4a) in replicative senescence of normal human fibroblasts. *Proceedings of the National Academy of Sciences of the United States of America*, 93(24): 13742–13747.

Chen Q. M., Tu V. C., Catania J., Burton M., Toussaint O., Dilley T., 2000. Involvement of Rb family proteins, focal adhesion proteins and protein synthesis in senescent morphogenesis induced by hydrogen peroxide. *J. Cell Sci.*, 113(22): 4087–4097.

Chen Y., Liu J., Yuan B., Cao C., Qin S., Cao X., Bian G., Wang Z., Jiang J., 2012. Methylated actinomycin D, a novel actinomycin D analog induces apoptosis in HepG2 cells through Fas- and mitochondria-mediated pathways. *Molecular Carcinogenesis*, 52(12): 983–996.

Da Silva-Álvarez S., Collado M., 2016. Encyclopedia of Cell Biology, Cellular Senescence. Academic Press, pp. 511–517.

Degan P., Cortese K., Pulliero A., Bruno S., Gagliani M. C., Congiu M., Izzotti A., 2021. Simulated Microgravity Effects on Human Adenocarcinoma Alveolar Epithelial Cells: Characterization of Morphological, Functional, and Epigenetic Parameters. *Int. J. Mol.*, 22(13): 6951.

Fischer M., 2017. Census and evaluation of p53 target genes. *Oncogene*, 36: 3943–3956.

Gire V., Dulić V., 2015. Senescence from G2 arrest, revisited. *Cell Cycle*, 14(3): 297–304.

González-Gualda E., Baker A. G., Fruk L., Muñoz-Espín D., 2021. A guide to assessing cellular senescence in vitro and in vivo. *FEBS J.*, 288(1): 56–80.

Grimm D., Wehland M., Corydon T. J., Richter P., Prasad B., Bauer J., Egli M., Kopp S., Lebert M., Krüger M., 2020. The effects of microgravity on differentiation and cell growth in stem cells and cancer stem cells. *Stem Cells Transl. Med.*, 9(8): 882–894.

- Hayflick L., Moorhead P. S., 1961. The serial cultivation of human diploid cell strains. *Exp. Cell Res.*, 25(3): 585–621.
- Ho C. N. Q., Tran M. T., Doan C. C., Hoang S. N., Tran D. H., Le L. T., 2021. Simulated Microgravity Inhibits the Proliferation of Chang Liver Cells by Attenuation of the Major Cell Cycle Regulators and Cytoskeletal Proteins. *Int. J. Mol. Sci.*, 22: 4550.
- Kumari R., Jat P., 2021. Mechanisms of Cellular Senescence: Cell Cycle Arrest and Senescence Associated Secretory Phenotype. *Front. Cell Dev. Biol.*, 9: 645593.
- Lei X., Cao Y., Zhang Y., Qian J., Zhao Q., Liu F., Zhang T., Zhou J., Gu Y., Xia G., Duan E., 2018. Effect of microgravity on proliferation and differentiation of embryonic stem cells in an automated culturing system during the TZ-1 space mission. *Cell Prolif.*, 51(5): e12466.
- Li F., Ye Y., Lei X., Zhang W., 2021. Effects of Microgravity on Early Embryonic Development and Embryonic Stem Cell Differentiation: Phenotypic Characterization and Potential Mechanisms. *Front. Cell Dev. Biol.*, 9: 797167.
- Li L., An L., Zhou X., Pan S., Meng X., Ren Y., Yang K., Guan Y., 2016. Biological behaviour of human umbilical artery smooth muscle cell grown on nickel-free and nickel-containing stainless steel for stent implantation. *Sci Rep*, 6: 18762.
- Martinelli L. K., Russomano T., Dos Santos M. A., Falcao F. P., Bauer M. E., Machado A., Sundaresan A., 2009. Effect of microgravity on immune cell viability and proliferation: simulation using 3-D clinostat. *IEEE Eng. Med. Biol. Mag.*, 28(4): 85–90.
- Mavrogonatou E., Konstantinou A. and Kletsas D. 2018. Long-term exposure to TNF- α leads human skin fibroblasts to a p38 MAPK- and ROS-mediated premature senescence. *Biogerontology*, 19(3–4): 237–249.
- Pathak R. U., Soujanya M., Mishra R. K., 2021. Deterioration of nuclear morphology and architecture: A hallmark of senescence and aging. *Ageing Res. Rev.*, 67: 101264.
- Quynh Chi H. N., Nghia Son H., Chinh Chung D., Huan L. D., Hong Diem T., Long L.T., 2020. Simulated microgravity reduces proliferation and reorganizes the cytoskeleton of human umbilical cord mesenchymal stem cells. *Physiol. Res.*, 69(5): 897–906.
- Sharpless N. E., Sherr C. J., 2015. Forging a signature of in vivo senescence. *Nat. Rev. Cancer*, 15: 397–408.
- Son H. N., Chi H. N. Q., Chung D. C., Long L. T., 2019. Morphological changes during replicative senescence in bovine ovarian granulosa cells. *Cell Cycle*, 18(13): 1490–1497.
- Stein G. H., Drullinger L. F., Soulard A., Dulić V., 1999. Differential roles for cyclin-dependent kinase inhibitors p21 and p16 in the mechanisms of senescence and differentiation in human fibroblasts. *Mol. Cell. Biol.*, 19(3): 2109–2117.
- van Deursen J. M., 2014. The role of senescent cells in ageing. *Nature*, 509(7501): 439–446.
- Vidyasekar P., Shyamsunder P., Arun R., Santhakumar R., Kapadia N. K., Kumar R., Verma R. S., 2015. Genome Wide Expression Profiling of Cancer Cell Lines Cultured in Microgravity Reveals Significant Dysregulation of Cell Cycle and MicroRNA Gene Networks. *PLoS One*, 10(8): e0135958.
- Wade Harper J., Adami G. R., Wei N., Keyomarsi K., Elledge S. J., 1993. The p21 Cdk-interacting protein Cip1 is a potent inhibitor of G1 cyclin-dependent kinases. *Cell*, 75: 805–816.
- Wang H. H., Lee Y. N., Su C. H., Shu K. T., Liu W. T., Hsieh C. L., Yeh H. I., Wu Y. J., 2020. S-Phase Kinase-associated Protein-2 Rejuvenates Senescent Endothelial Progenitor Cells and Induces Angiogenesis in Vivo. *Sci. Rep.*, 10: 6646.